Prediction and Measurement Techniques for Radiated EMI of Power Converters with Cables

Zhedong Ma and Shuo Wang[*]

(Power Electronics and Electrical Power Research Lab, University of Florida, 32611 USA)

Abstract: Recently, radiated electromagnetic interference (EMI) has become a research hotspot in power electronics systems, as the switching frequencies of power electronics systems have increased significantly with the adoption of wide-bandgap devices. In this article, a generalized radiated EMI model for power electronics converters with power cables is first reviewed. The radiated EMI model is then developed for a flyback power converter with critical ground impedance included. Based on the developed model, accurate high-frequency parameter extraction techniques and a radiated EMI prediction technique are developed and experimentally validated. Finally, essential measurement techniques are identified and developed to accurately extract parameters for accurate EMI prediction. The effects of the resolution bandwidth of the spectrum analyzer and critical PCB ground impedance on the radiated EMI are experimentally validated. PCB's impact on the common-mode (CM) choke's impedance and the radiated EMI is further validated. Techniques for minimizing the undesired near-field couplings in parameter extraction are discussed. The predicted EMI properly agreed with the measured EMI in the range of 30-230 MHz based on the EN55032 3 m class B standard.

Keywords: Radiated electromagnetic interference, power converters, power cables, spectrum analyzer, resolution bandwidth

1 Introduction

Within the last two decades, particularly with the adoption of wide-bandgap semiconductor devices, the switching speed and switching frequencies of power conversion systems have significantly increased to achieve high power densities [1-3]. However, high switching speeds and high frequencies have generated high electromagnetic interference (EMI) not only in the conventional conductive EMI frequency range but also in radiated EMI frequency range, which has not been fully investigated. Existing research mostly focuses on the modeling, measurement, and suppression of conducted EMI below 30 MHz [4-5]. For the conducted EMI, the EMI noise can be modeled and measured with differential-mode (DM) and common-mode (CM) EMI [6-8]. However, the radiated EMI of power electronics has seldom been investigated in recent years [9].

For radiated EMI analysis, the input and output cables of the power converter can be represented with an undesired antenna, as shown in Fig. 1a. An undesired antenna can be modeled with the antenna impedance Z_A.

$$Z_A = R_r + R_L + jX_A \tag{1}$$

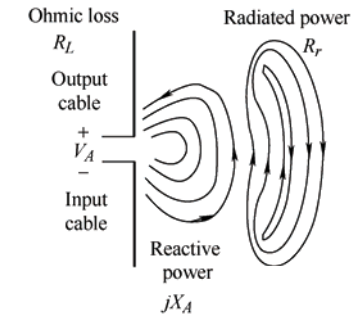

(a) Cable antenna model

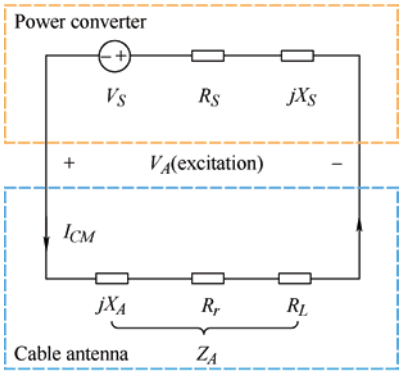

(b) Radiated EMI model

Fig. 1 A generalized radiated EMI model with cables

Manuscript received November 5, 2022; revised November 20, 2022; accepted November 27, 2022. Date of publication December 31, 2022; date of current version December 8, 2022.
*Corresponding Author, E-mail: shuowang@ieee.org
Digital Object Identifier: 10.23919/CJEE.2022.000033

In Eq. (1) and Fig. 1, R_r represents the energy radiated to the free space. R_L represents the resistance of the power cables. X_A represents the near-field energy between two cables [10].

The switching-mode power converter can be represented with Thevenin equivalence: a noise voltage source V_S in series with a source impedance $R_s + jX_s$, as shown in Fig. 1b. The excitation voltage V_A across the cable antenna drives the antenna, leading to CM currents for EMI radiation [11]. Radiated EMI is mainly caused by the CM currents flowing on the input and output cables unless the power converter has very high switching currents and very large DM noise current loops [12].

In isolated power converters with power cables, V_A is the voltage difference between the primary ground and the secondary ground, which is mainly caused by the unbalanced parasitics of the transformer [13-14]. In non-isolated power converters with power cables, V_A is the voltage difference across the input and output cables owing to the noise current voltage drop on the ground impedance [15].

To mitigate the radiated EMI, a high-frequency CM choke can be designed to suppress [16], and a high-frequency Y-capacitor can be designed to bypass the CM currents flowing through the cable antenna [16]. Shielding techniques are also widely implemented to solve the near-field coupling issues between EMI filters, transformers, and the attached power cables [17-18]. Transformer shielding winding and cancellation winding techniques were developed to significantly reduce the CM noise [19-20]. The critical ground impedance was identified and minimized to reduce the undesired transformation from the DM currents to the CM excitation voltage V_A [15, 21].

Jia et al. [22] predicted the radiated EMI based on the superposition of the electric field generated by the distributed Hertzian dipole current along the power cables. Gao et al. [23] and Chen et al. [24] predicted the far-field radiated EMI based on near-field scanning. In contrast to existing studies, this article predicts the radiated EMI based on the radiated EMI model for power converters in Fig. 1b and the measurements. An active-clamp flyback power converter is used to demonstrate the developed technology. The modeling, measurement, and prediction techniques were developed and experimentally validated.

The remainder of this article is organized as follows. In Section 2, the radiated EMI model for a flyback converter with power cables was developed. In Section 3, a technique to predict the radiated EMI based on the developed radiated EMI model and measurements was developed and experimentally validated. In Section 4, essential measurement techniques to accurately predict the radiated EMI were discussed and experimentally validated. Finally, Section 5 concluded the article.

2 Radiated EMI model for a flyback power converter with power cables

Fig. 2a shows the circuit topology of the flyback converter with power cables under investigation, and Fig. 2b shows the experiment setup for radiated EMI measurement in a 3 m semi-anechoic chamber based on the EN55032 class B standard. In the experiments, the AC excitation is 120 V/60 Hz, the DC output is 20 V, the switching frequency of the flyback converter is 125 kHz, and the load is a 6.16 Ω power resistor. A 0.8 m input cable was connected between the input of the flyback adapter and the AC line. A 2 m output cable (type C) was connected between the flyback adapter and the load resistor. Ferrite beads were applied to the input cable on the ground to eliminate the coupling between the AC line and the input cable (0.8 m) as well as the output cable (2 m).

In Fig. 2a, a CM choke L_{CM} was applied before the diode bridge for CM current suppression, a Y-capacitor was deployed between the PGND and SGND to bypass the CM current flowing through the input and output cables. Transformer shielding and cancellation windings have been designed and optimized to reduce the CM noise.

The impedances of the bulk capacitor C_{DC}, X-capacitor C_X, and output capacitor C_{out} are assumed to be zero for CM EMI analysis [13]. The impedances of the diode rectifier and the DM inductor L_{DM} can be ignored for radiated EMI analysis because they are much smaller than the Z_A of the cable antenna [13]. The transformer can be represented by a two-impedance

model for CM EMI analysis [25]. Based on the substitution theory [26], semiconductor switches can be replaced with voltage or current sources, which have the same voltage or current waveforms as the switches to be replaced, for EMI analysis. Thus, in Fig. 2a, S1 is replaced with a voltage source, S2 and S3 are replaced with current sources, and a detailed analysis is provided in Ref. [13]. A radiated EMI model of the flyback converter under investigation is therefore developed in Fig. 3 [21].

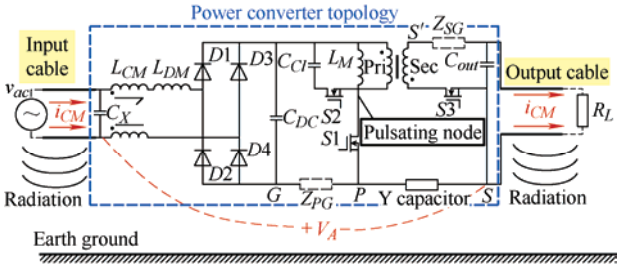

(a) Circuit topology of the flyback converter under investigation

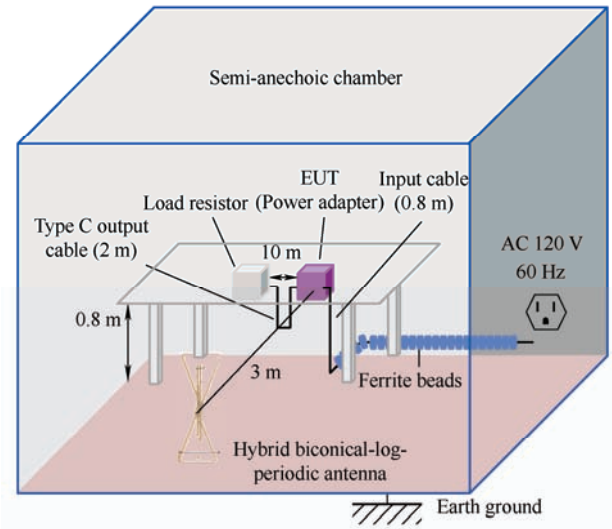

(b) Experimental setup for radiated EMI measurement under the EN55032 class B 3 m standard

Fig. 2 A flyback converter for radiated EMI measurement

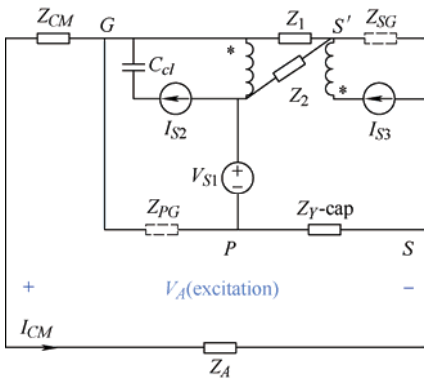

Fig. 3 A radiated EMI model for the flyback converter with power cables under investigation

In Fig. 3, Z_{CM} represents the CM choke impedance; Z_1 and Z_2 represent the two-impedance model of the transformer; $Z_{Y\text{-cap}}$ represents the Y-capacitor impedance. V_A is the equivalent voltage excitation that drives the cable antenna for EMI radiation as defined previously. Z_{PG} and Z_{SG} represent the critical ground impedance on the primary and secondary sides of the power converter, respectively, whose impact on radiated EMI will be analyzed and validated later.

3 Radiated EMI prediction

The proposed flowchart for predicting radiated EMI is shown in Fig. 4. This article predicts the radiated EMI from 30 MHz to 230 MHz as the EN55032 3 m class B standard has the strictest radiated EMI limit in this range.

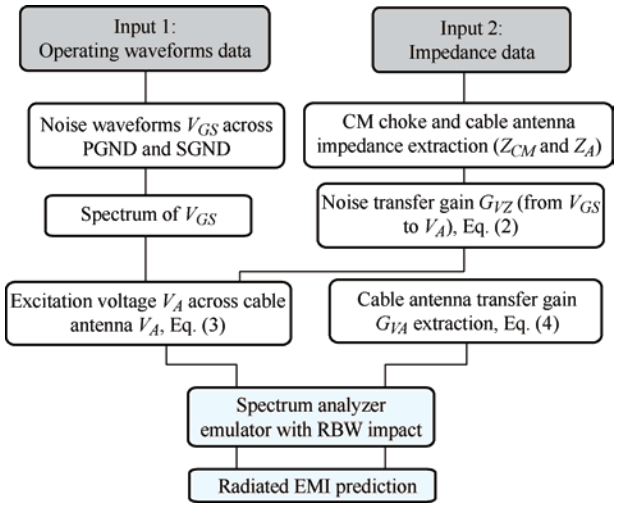

Fig. 4 Flowchart for radiated EMI prediction

3.1 V_{GS} extraction

Based on the work in Refs. [15, 21], the critical ground impedance (certain PCB ground trace inductance) in power converters is crucial in radiated EMI. Therefore, the critical ground impedance Z_{PG} and Z_{SG} in Fig. 3 must be included in the extraction of V_{GS} (voltage between nodes G and S in Fig. 3) across PGND and SGND. The measured V_{GS} is shown in Fig. 5a, whereas the fast Fourier transform (FFT) spectrum is shown in Fig. 5b. The oscilloscope used in the measurements was a Rigol MSO4054 with a 500 MHz bandwidth, whereas the probe was a Rigol RP3500 A with a 500 MHz bandwidth.

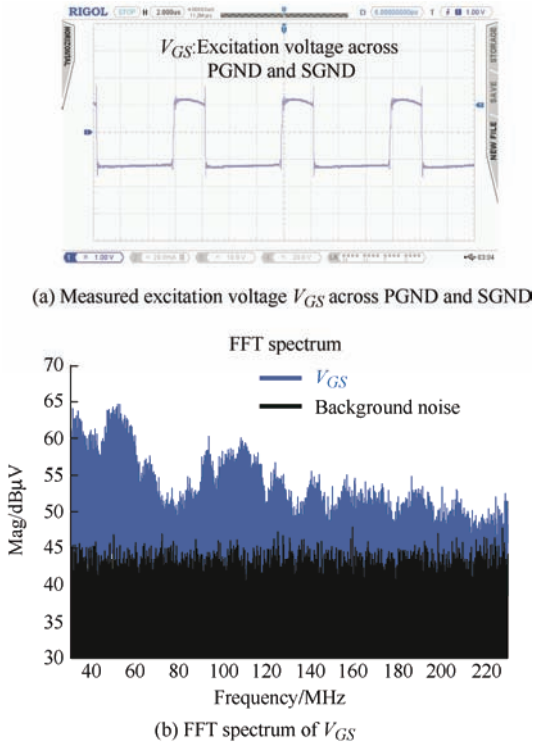

Fig. 5 Excitation voltage and its FFT spectrum

3.2 Impedance extraction

The impedance Z_{CM} of the CM choke and Z_A of the cable antenna were extracted with S-parameters using a Copper Mountain planar 808/1 vector network analyzer (VNA) [27]. They are shown in Fig. 6. It should be noted that the Z_{CM} should be measured with the choke on the PCB to include PCB's impact on Z_{CM}.

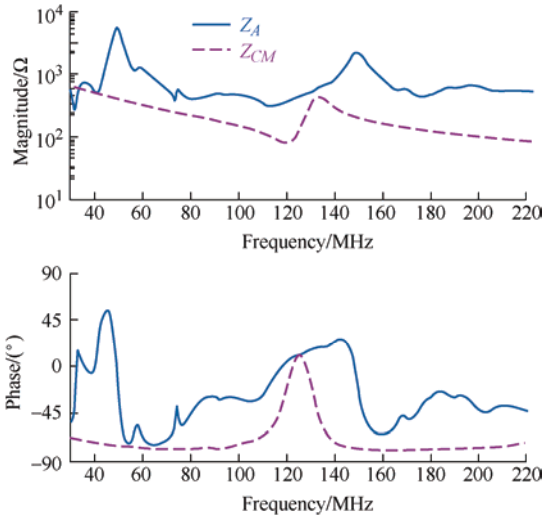

Fig. 6 Impedance curves for the CM choke Z_{CM} and cable antenna Z_A

3.3 Noise transfer gain prediction

Based on the impedance curves of Z_{CM}, Z_A, and Fig. 3, the noise transfer function G_{VZ} from V_{GS} to V_A can be predicted using Eq. (2) and is shown in Fig. 7.

$$G_{VZ} = \frac{Z_A}{Z_A + Z_{CM}} \tag{2}$$

Furthermore, the excitation voltage V_A across the cable antenna can be predicted using Eq. (3). Z_{CM} and Z_A should be accurately extracted to accurately predict G_{VZ}, V_A, and the radiated EMI.

$$V_A = V_{GS} \cdot G_{VZ} \tag{3}$$

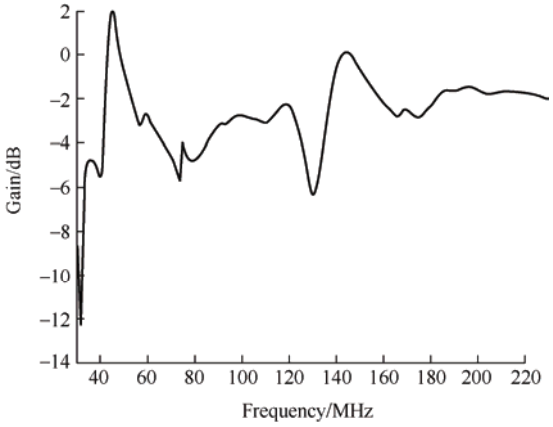

Fig. 7 The predicted noise transfer function G_{VZ}

3.4 Cable antenna gain extraction

The radiated power P_r on R_r can be predicted based on the model shown in Fig. 3. The antenna transfer function G_{VA} from $|V_A|$ to the radiated maximum electric field intensity $E_{\max}$ at distance r from the power converter is expressed as follows [21]

$$G_{VA} = \frac{E_{\max}}{|V_A|} = \sqrt{\frac{1}{2}\left[\frac{R_r}{|R_L + R_r + jX_A|^2}\right]\frac{\eta D_o}{\pi r^2}} \tag{4}$$

where η is the characteristic impedance of 120π Ω and D_o is the maximum directivity of the antenna at distance r.

To extract the gain of the cable antenna in the semi-anechoic chamber, the flyback adapter in Fig. 2b is replaced with an RF signal generator (Rigol DSG830) as shown in Fig. 8, the flyback adapter was removed from the intact cables. The terminals of the two conductors of the cables were shorted on the converter sides. The excitation voltage generated from the RF generator is added to the cable terminals where the flyback adapter was originally connected through a wideband unbalance-to-balance transformer (FTB-1-1*A15, effective frequency range: 0.2-500 MHz). High-frequency ferrite beads were added to the output cable of the RF signal generator and the output cable of the transformer to minimize their coupling to

the cable antenna. E_{max} was measured using a receiving antenna (SUNAR RF MOTION JB3) 3 m away as in Fig. 8 [28].

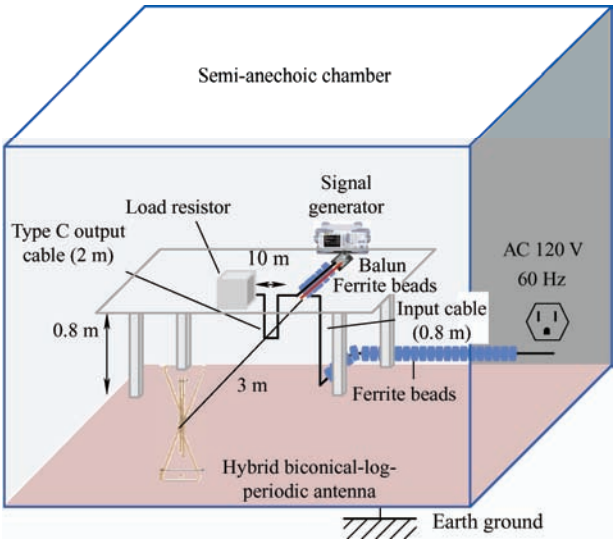

Fig. 8 Experimental setup for extracting antenna's gain G_{VA}

To extract the cable antenna's gain from 30 MHz to 230 MHz, 5 MHz and 10 MHz square-wave voltage excitations generated from the RF signal generator were fed to the cable antenna. The voltage across the input and output cable is measured and shown in Fig. 9a (due to the limited space, only the 10 MHz excitation is shown here). The FFT spectrum is shown in Fig. 9b, whereas the measured radiated

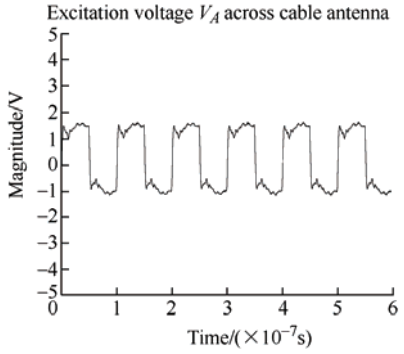

(a) A 10 MHz suqare-wave excitation voltage was added across the cable antenna

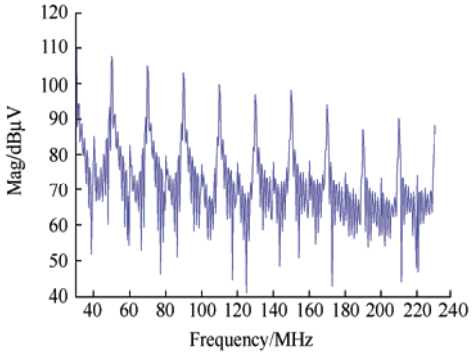

(b) FFT spectrum of Fig. 9a

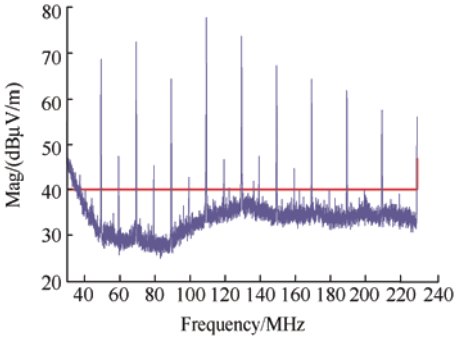

(c) Measured radiated EMI spectrum in Fig. 9a

Fig. 9 Excitation voltage added across the cable antenna and its FFT, and the measured radiated EMI spectrum

EMI is shown in Fig. 9c. Notably, a 20 dB attenuator is applied to protect the spectrum analyzer; thus, the background noise in Fig. 9c is above 20 dB.

The cable antenna gain can be derived from Tab. 1 at different harmonic frequencies for the case of 10 MHz square-wave excitation. The gain for the case of the 5 MHz square-ware excitation is derived similarly.

Tab. 1 Extracted antenna gain

Frequency /MHz	Excitation voltage/dBμV	E-field /(dBμV/m)	Antenna gain/dB
30	110.8	55.06	–55.74
50	108.5	68.41	–40.09
70	105.7	72.21	–33.49
90	103.8	64.10	–39.70
110	100.5	74.60	–25.90
130	97.79	73.47	–24.32
150	98.98	67.06	–31.92
170	94.87	64.04	–30.83
190	87.84	61.56	–26.28
210	91.01	57.41	–33.60
230	89.36	55.71	–33.65

In Tab. 1, only the gains at odd-order harmonic frequencies were derived because the square wave with a 50% duty cycle has zero even-order harmonics. By interpolating the derived gains for the 5 MHz and 10 MHz excitation cases at different harmonic frequencies, the extracted gain G_{VA} is shown in Fig. 10. It has bumps at approximately 70 MHz, 110 MHz, 130 MHz, and 200 MHz, and these bumps may result in radiated EMI spikes.

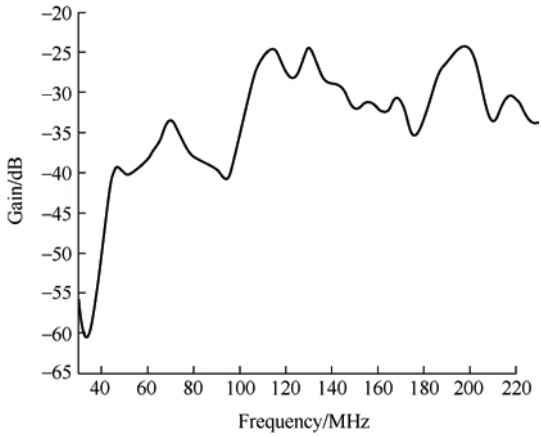

Fig. 10 Extracted antenna gain G_{VA}

3.5 Radiated EMI prediction

The radiated EMI can be predicted based on Figs. 6-7, 10, and Eq. (5)

$$E = |V_{GS} \cdot G_{VZ}| \cdot G_{VA} \tag{5}$$

Based on the theory developed in Ref. [29], spectrum analyzers operate differently from FFT. FFT calculates the magnitude of each harmonic order. Conversely, the operating principle of the spectrum analyzer is shown in Fig. 11. The spectrum analyzer first sweeps the frequencies by changing the frequency of the local oscillator. The mixer converts the harmonics at the swept frequencies into signals at a fixed intermediate frequency (IF). The converted harmonics, including those lower or higher than IF, are processed via an IF filter which has a −6 dB resolution bandwidth (RBW). In the EMI standard EN55032, the RBW is 120 kHz from 30 MHz to 1 GHz. Based on Ref. [29], when more than one harmonic is located within 2RBW, depending on their phases, these harmonics can stack up in the time domain at the output of the IF filter. The envelope detector catches the increased amplitude and feeds it to the peak, quasi-peak, and average EMI detectors. The measured EMI noise could therefore be higher than individual harmonics. For the case under investigation, the switching frequency is 125 kHz; therefore, two orders of harmonics exist within 2RBW (240 kHz). The measured EMI noise via a spectrum analyzer with 120 kHz RBW will be therefore higher than the FFT result.

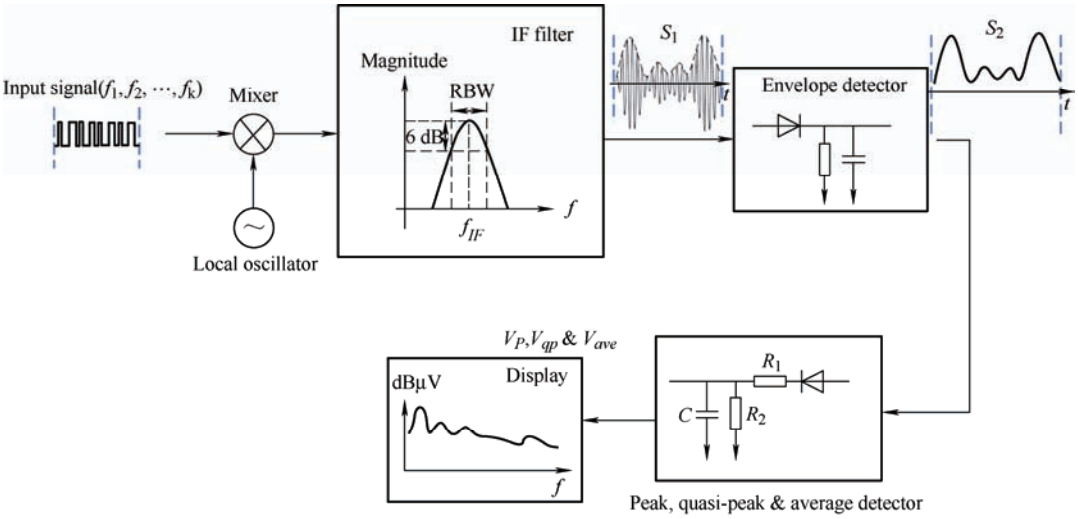

Fig. 11 Operating principle of a spectrum analyzer

The radiated EMI predicted using the spectrum analyzer emulator developed in Ref. [29] (RBW's impact is considered) is compared with both the measured and predicted EMI with FFT (RBW's impact is not considered) in Fig. 12. The predicted EMI from the spectrum analyzer emulator is in good agreement with the measured EMI from 30 MHz to 230 MHz. The big difference below 40 MHz results from background noise. On the other hand, the FFT result is 6-8 dB lower than the measured and predicted EMI from the spectrum analyzer emulator.

The bump of G_{VZ} at 45 MHz in Fig. 7 leads to the EMI spike, as shown in Fig. 12. The EMI spikes at 70 MHz, 110 MHz, 130 MHz, and 200 MHz in Fig. 12 resulted from the bumps of the cable antenna's gain G_{VA} in Fig. 10. The highest radiated EMI spike around 110 MHz is caused by both the bumps of G_{VA} and the high voltage spectrum (V_{GS}) at 110 MHz. The above analysis indicates V_{GS}, G_{VZ}, and G_{VA} are critical for the radiated EMI.

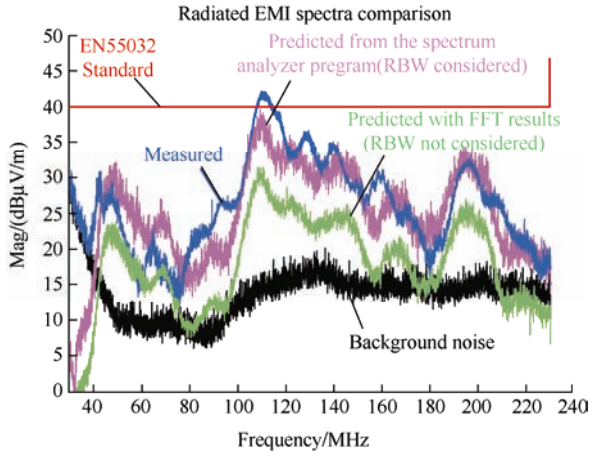

Fig. 12 Comparison of the measured and predicted radiated EMI spectra

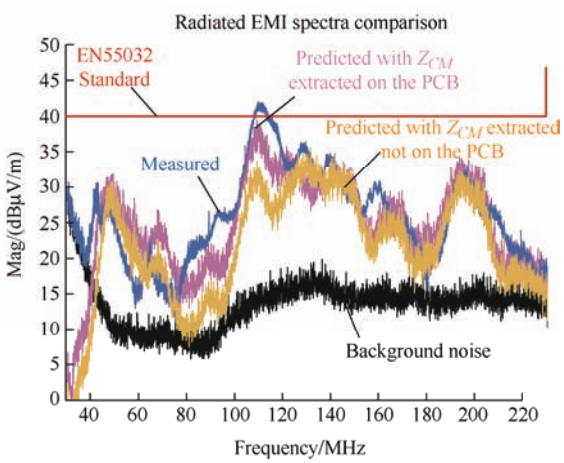

(b) Comparison of predicted EMI

Fig. 13 Influence of the CM choke impedance on radiated EMI

4 Measurement techniques for radiated EMI prediction

To accurately predict radiated EMI, numerous issues should be considered, from data processing to measurement techniques.

(1) The impedance of the CM choke should be extracted with the CM choke remaining on the PCB; otherwise, the influence of the PCB will not be reflected in the impedance curve, which will influence the prediction of the noise transfer function G_{VZ} and finally lead to errors in the predicted EMI spectrum. The extracted Z_{CM} on the PCB and not on the PCB are shown in Fig. 13a, whereas the predicted radiated EMI in these two cases is shown in Fig. 13b. The influence of the PCB on Z_{CM} can lead to a 5 dB error in the final predicted radiated EMI. Notably, all measurements were conducted in the EMC chamber; thus, all undesired external disturbances were eliminated. SMA RF connectors were used to connect the VNA to the PCB for impedance measurements.

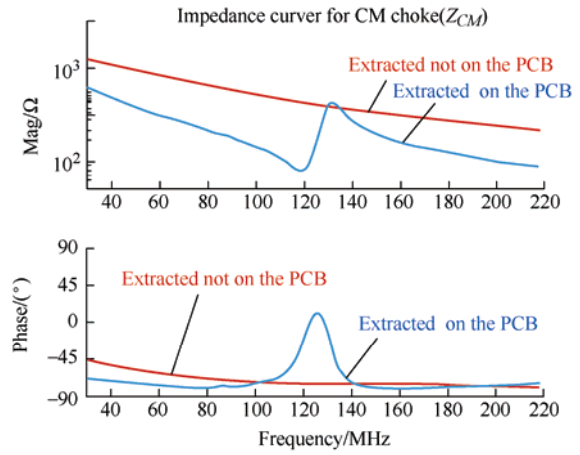

(a) Z_{CM} curves extracted on PCB versus those extracted not on PCB

(2) The radiation from the AC input power cable of the signal generator should be minimized by applying lossy high-frequency ferrite beads, as shown in Fig. 14. The AC power cable can radiate significant EMI, compromising the accuracy of the extracted G_{VA} in Fig. 8.

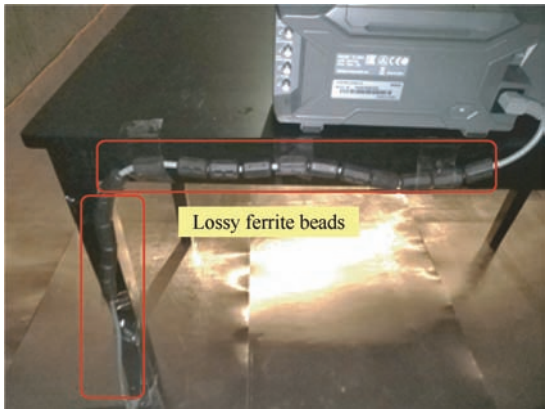

Fig. 14 Lossy ferrite beads applied to the AC input power cable to reduce the undesired radiation

In addition, ferrite beads should be applied to the input power cable of the converter under investigation on the ground and the coaxial cables connected to the network analyzer for antenna impedance Z_A measurement, as shown in Fig. 15. This is to eliminate undesired couplings from the AC line and minimize the couplings between coaxial cables, the input cable (0.8 m), and the output cable (2 m) [25]. This is crucial because an inaccurate Z_A results in inaccurate G_{VZ} prediction, finally leading to inaccurate EMI spectrum prediction.

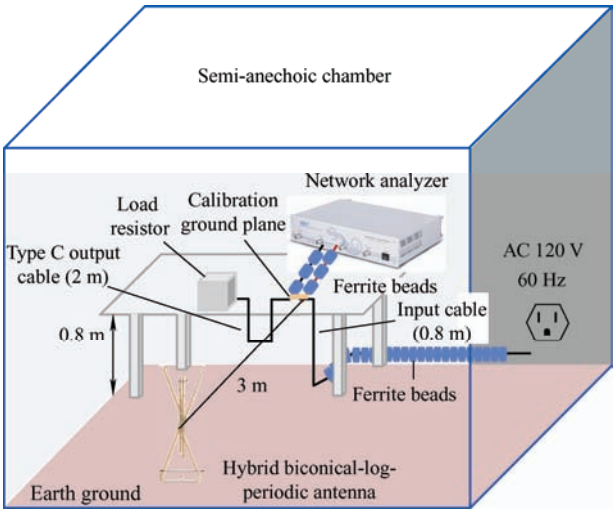

Fig. 15 Ferrite beads applied to the coaxial cables connected to the network analyzer and the power converter's input cable for impedance measurement

(3) Only if the switching frequency of the power converter is fixed and bigger than 2RBW (240 kHz for EN 55032 standard), the FFT can be directly used for radiated EMI prediction.

If the switching frequency of the power converter is smaller than 240 kHz, or the switching frequency varies, the RBW's impact on the measured radiated EMI should be considered. The developed spectrum analyzer emulator should be used for the radiated EMI prediction [29]. Without including the impact of RBW, FFT can have up to 35 dB [30] difference from the measured.

(4) Because the impedance of critical PCB traces cannot be ignored above 30 MHz [15, 21] for radiated EMI analysis, the impact of critical PCB traces must be included when extracting the voltage in power converters. A comparison of the FFT spectra of voltages with (V_{GS}) and without (V_{PS}) the influence of the critical ground impedance is shown in Fig. 16a. The predicted radiated EMI spectra with and without the influence of the critical ground impedance are shown in Fig. 16b. The critical ground impedance has an impact of up to 10 dB on the radiated EMI for the case under investigation.

The critical ground impedance in isolated power converters was identified in Ref. [31], whereas that in non-isolated power converters was identified in Ref. [15].

Identification of the critical ground impedance.

(1) Discontinuous currents flow through the ground impedance; therefore, a high di/dt results in a high-frequency voltage drop on the ground impedance above 30 MHz.

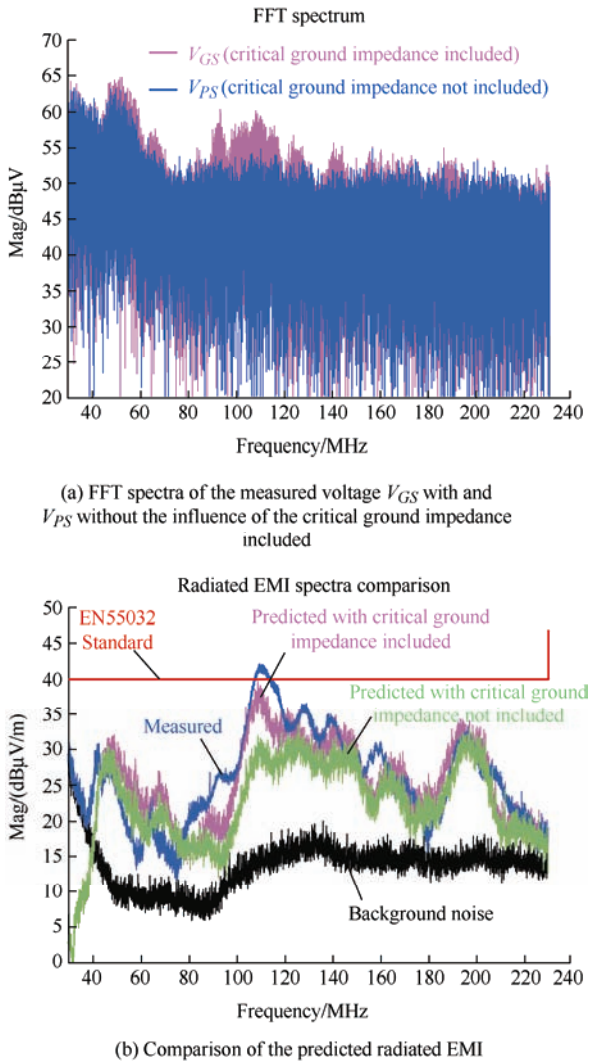

(a) FFT spectra of the measured voltage V_{GS} with and V_{PS} without the influence of the critical ground impedance included

(b) Comparison of the predicted radiated EMI

Fig. 16 Influence of the critical ground impedance on radiated EMI

(2) The voltage drop on the ground impedance is in series with those on the other components (for example, the Y-capacitor and CM inductors) across the input and output cables. In other words, these voltage drops are part of the excitation voltage that drives the cable antenna for EMI radiation.

5 Conclusions

In this article, the modeling, measurement, and prediction techniques for a flyback converter with power cables were investigated and experimentally validated. The contributions of the article are as follows.

(1) Developed a radiated EMI model with critical

ground impedance included for Flyback converters with power cables.

(2) Developed and experimentally validated radiated EMI prediction and accurate parameter extraction techniques based on the developed radiated EMI model and measurements.

(3) Explored how the radiated EMI spikes are related to the noise voltage, impedances, and cable antenna's gain.

(4) Identified and developed important measurement techniques to accurately extract parameters for the radiated EMI prediction.

(5) The influence of the RBW of the spectrum analyzer on the measured and predicted radiated EMI was validated.

References

[1] B Zhang, S Wang. A survey of EMI research in power electronics systems with wide-bandgap semiconductor devices. *IEEE J. Emerg. Sel. Topics Power Electron.*, 2020, 8(1): 626-643.

[2] H Li, X Zhao, W Su, et al. Nonsegmented PSpice circuit model of GaN HEMT with simulation convergence consideration. *IEEE Trans. Ind. Electron.*, 2017, 64(11): 8992-9000.

[3] Y Zhang, S Wang, Y Chu. Analysis and comparison of the radiated electromagnetic interference generated by power converters with Si MOSFETs and GaN HEMTs. *IEEE Trans. Power Electron.*, 2020, 35(8): 8050-8062.

[4] Z Wang, H Li, Z Chu, et al. A review of EMI research in modular multilevel converter for HVDC applications. *IEEE Trans. Power Electron.*, 2022, 37(12): 14482-14498.

[5] H Zhang, S Wang, Y Li, et al. Two-capacitor transformer winding capacitance models for common-mode EMI noise analysis in isolated DC-DC converters. *IEEE Trans. Power Electron.*, 2017, 32(11): 8458-8469.

[6] Z Zhang, Y Hu, X Chen, et al. A review on conductive common-mode EMI suppression methods in inverter fed motor drives. *IEEE Access*, 2021, 9: 18345-18360.

[7] Y Li, H Zhang, S Wang, et al. Investigating switching transformers for common mode EMI reduction to remove common mode EMI filters and Y-capacitors in flyback converters. *IEEE J. Emerg. Sel. Topics Power Electron.*, 2018, 6(4): 2287-2301.

[8] J Yao, Y Li, Z Ma, et al. Advances of modeling and reduction of conducted and radiated EMI in flyback converters. *Proc. IEEE Energy Convers. Congr. Expo.*, October 11-15, 2022, Detroit, MI, USA. IEEE, 2020: 3362-3369.

[9] J Yao, Z Ma, Y Lai, et al. A survey of modeling and reduction techniques of radiated EMI in power electronics. *2021 IEEE International Joint EMC/SI/PI and EMC Europe Symposium*, 2021: 1081-1086.

[10] C A Balanis. Antenna theory: Analysis and design. 3rd ed. Hoboken: Wiley, 2016.

[11] Y Zhang, S Wang, Y Chu. Investigation of radiated electromagnetic interference for an isolated high-frequency DC-DC power converter with power cables. *IEEE Trans. Power Electron.*, 2019, 34(10): 9632-9643.

[12] J Yao, Y Lai, Z Ma, et al. Advances in modeling and reduction of conducted and radiated EMI in non-isolated power converters. *Proc. IEEE Appl. Power Electron. Conf. Expo.*, June 14-17, 2021, Phoenix, AZ, USA. IEEE, 2021: 2305-2312.

[13] J Yao, Y Li, S Wang, et al. Modeling and reduction of radiated EMI in a GaN IC-based active clamp flyback adapter. *IEEE Trans. Power Electron.*, 2021, 36(5): 5440-5449.

[14] J Yao, Y Lai, Z Ma, et al. Investigation of noise spectrum and radiated EMI in high switching frequency flyback converters. *Proc. IEEE Appl. Power Electron. Conf. Expo.*, June 14-17, 2021, Phoenix, AZ, USA. IEEE, 2021: 2265-2270.

[15] J Yao, S Wang, Z Luo. Modeling, analysis, and reduction of radiated EMI due to the voltage across input and output cables in an automotive non-isolated power converter. *IEEE Trans. Power Electron.*, 2022, 37(5): 5455-5465.

[16] Y Zhang, S Wang. Characterization and design of filter inductors and capacitors to suppress the radiated EMI in a power converter. *2022 International Power Electronics Conference (IPEC-Himeji 2022- ECCE Asia)*, 2022: 1082-1089.

[17] Y Li, S Wang, H Sheng, et al. Investigate and reduce capacitive couplings in a flyback adapter with a DC-bus filter to reduce EMI. *IEEE Trans. Power Electron.*, 2020, 35(7): 6963-6973.

[18] Z Ma, J Yao, S Wang, et al. Radiated EMI reduction with double shielding techniques in active-clamp flyback converters. *2021 IEEE International Joint EMC/SI/PI and EMC Europe Symposium*, July 26-August 13, 2021, Raleigh, NC, USA. IEEE, 2021: 1064-1069.

[19] H Chen, C Zhao, Z Zheng. Design of the number of transformer shielding winding turns for minimizing low-frequency common-mode noise in flyback converters. *IEEE Trans. Electromagn. Compat.*, 2019, 61(6): 1961-1966.

[20] H Chen, Z Zheng, J Xiao. Determining the number of transformer shielding winding turns for suppressing common-mode noise in flyback converters. *IEEE Trans. Electromagn. Compat.*, 2018, 60(5): 1606-1609.

[21] Z Ma, S Wang, H Sheng, et al. Modeling and reduction of radiated EMI due to ground impedance in a high-density active-clamp flyback power adapter. *2022 IEEE Appl. Power Electron. Conf. Expo.*, March 20-24, 2022, Houston, TX, USA. IEEE, 2022: 292-299.

[22] J Jia, D Rinas, S Frei. Predicting the radiated emissions of automotive systems according to CISPR 25 using current scan methods. *IEEE Trans. Electromagn. Compat.*, 2016, 58(2): 409-418.

[23] X Gao, J Fan, Y Zhang, et al. Far-field prediction using only magnetic near-field scanning for EMI test. *IEEE Trans. Electromagn.Compat.*, 2014, 56(6): 1335-1343.

[24] H Chen, T Wang, L Feng, et al. Determining far-field EMI from near-field coupling of a power converter. *IEEE Trans. Power Electron.,* 2014, 29(10): 5257-5264.

[25] J Yao, S Wang, H Zhao. Measurement techniques of common mode currents, voltages, and impedances in a flyback converter for radiated EMI diagnosis. *IEEE Trans. Electromagn. Compat.*, 2019, 61(6): 1997-2005.

[26] Y Chu, S Wang. A generalized common-mode current cancelation approach for power converters. *IEEE Trans. Power Electron.*, 2015, 62(7): 4130-4140.

[27] S Wang, F C Lee, W G Odendaal. Characterization and parasitic extraction of EMI filters using scattering parameters. *IEEE Trans. Power Electron*., 2005, 20(2): 502-510.

[28] Z Ma, Y Yang, J Yao, et al. Radiated EMI prediction in power converters with power cables based on cable antenna voltage gain extraction. *2022 IEEE International Symposium on Electromagnetic Compatibility & Signal/Power Integrity* (*EMCSI*), August 1-5, 2022, Spokane, WA, USA. IEEE, 2022: 510-515.

[29] L Yang, S Wang, H Zhao, et al. Prediction and analysis of EMI spectrum based on the operating principle of EMC spectrum analyzers. *IEEE Trans. Power Electron.*, 2020, 35(1): 263-275.

[30] Z Ma, Y Li, S Wang, et al. Investigation and reduction of EMI noise due to the reverse recovery currents of 50/60 Hz diode rectifiers. *IEEE J. Emerg. Sel. Topics Ind. Electron.*, 2022, 3(3): 594-603.

[31] Z Ma, S Wang, H Sheng, et al. Modeling, analysis and mitigation of radiated EMI due to PCB ground impedance in a 65W high-density active-clamp flyback converter. *IEEE Transactions on Industrial Electronics*, 2022, 37(5): 5455-5465.

Zhedong Ma received the B.Eng. degree in Electrical Engineering and Automation from Zhejiang University, Hangzhou, China, in 2019. He is currently working toward the Ph.D. degree in Electrical and Computer Engineering at the University of Florida, Gainesville, FL, USA.

His research interests include electromagnetic interference/ compatibility (EMI/EMC) in power electronics systems, magnetic components, and wireless charging. He has authored and coauthored more than 16 IEEE journal and conference papers and holds one US patent pending since 2019.

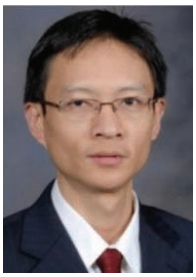

Shuo Wang (Fellow, IEEE) received the Ph.D. degree in Electrical Engineering from Virginia Tech, Blacksburg, VA, USA, in 2005.

He is currently a Full Professor with the Department of Electrical and Computer Engineering, University of Florida, Gainesville, FL, USA. He has authored or coauthored more than 200 IEEE journal and conference papers and holds around 30 pending/issued U.S./international patents.

Dr. Wang was the recipient of the Best Transaction Paper Award from the IEEE Power Electronics Society in 2006 and two William M. Portnoy Awards for the papers published in the IEEE Industry Applications Society in 2004 and 2012, and the Distinguished Paper Award from the 2022 IEEE Symposium on Security and Privacy. In 2012, he was also the recipient of the National Science Foundation Career Award. He is currently an Associate Editor for the IEEE Transactions on Industry Applications and the IEEE Transactions on Electromagnetic Compatibility. He is the Chair of Power Electronics EMI/EMC Special Committee of IEEE EMC Society and an Instructor of IEEE Clayton Paul Global University. He was a Technical Program Co-Chair of the IEEE 2014 International Electric Vehicle Conference.